RSC Advances

PAPER

View Article Online
View Journal | View Issue

CrossMark click for updates

Cite this: *RSC Adv.*, 2017, **7**, 6486

Preparation of highly porous carbon through activation of NH_4Cl induced hydrothermal microsphere derivation of glucose†

Chunyan Zhang, Shuang Lin, Junjun Peng, Yanzhong Hong, Zhiyong Wang and Xianbo Jin*

Received 1st November 2016
Accepted 3rd January 2017

DOI: 10.1039/c6ra26141h

www.rsc.org/advances

There is considerable interest in the synthesis of activated carbons from biomass through hydrothermal carbonization (HTC) followed by activation. Here we report our findings that using NH_4Cl additive for HTC of glucose changes the product from nanosphere carbon to N-doped microsphere carbon with a much lower surface area, but unexpectedly, the following KOH-activated N-doped microsphere carbon shows a significantly higher specific surface area (exceeding 3000 $m^2\ g^{-1}$) than that (2385 $m^2\ g^{-1}$) of activated conventional HTC carbon. Under similar conditions, other HTC additives, such as NaCl and HCl, can also lead to the formation of microsphere carbons with decreased surface area, but the specific surface area of the corresponding activated carbons decreased accordingly. These comparisons together with XPS and FTIR analyses suggest that the doped N in the HTC carbon play an important role on the formation of extra pores during the activation. Furthermore, the activated N-doped microsphere carbon delivers the highest specific capacity (349 F g^{-1}) at a current density of 1 A g^{-1} in 6 mol L^{-1} KOH. Our findings promise an efficient route to the preparation of N-doped highly porous carbon with high capacitive performance.

Open Access Article. Published on 19 January 2017. Downloaded on 1/19/2026 6:30:39 PM. This article is licensed under a Creative Commons Attribution 3.0 Unported Licence.

1 Introduction

Activated carbons (ACs) have found a large number of applications in the environment and energy fields.[1,2] Their extensive microporous structure and high specific surface areas (2000–3000 $m^2\ g^{-1}$) make the ACs highly demanded by industry as adsorbents for water and air purification,[3–6] and electrode materials for supercapacitors.[7,8] The worldwide market of ACs is increasing by nearly 10% per year, and the global annual consumption will reach about 1.65 Mt in 2017.[9] Developing simple processes for the preparation of high performance ACs is of great significance.

ACs can be regarded as abundant in natural resources, because they can be derived from biomass through carbonization followed by activation. Hydrothermal carbonization (HTC) is a well-established route to convert biomass, including carbohydrates and lignocelluloses, to carbon materials.[10–13] Particularly, HTC of monosaccharide (such as glucose[14]) and oligosaccharides (such as sucrose[15]) have been well studied. But just like high temperature carbonization processes,[16] HTC generates carbons with very low specific surface areas. A following high temperature activation with H_2O, CO_2 or KOH is essential for the HTC carbons to be used as high performance absorbents or supercapacitor materials.[17–20]

Previously, many organic and inorganic additives for the HTC process have been studied, aiming at synthesis of HTC carbons with different morphologies and compositions. Some additives can decrease the specific surface area of the HTC carbons. For example, while HTC of glucose in water results in carbon nanopowders with particle sizes of about 200 nm,[21,22] adding sodium borate into the HTC reactor could lead to finer carbon with particle sizes to about 50 nm.[23] A further decrease of the particle size to about 10 nm HTC carbon has been realized by using $ZnCl_2$ based additives mixtures,[24] and the resulting HTC carbon has a relatively high specific surface area of about 650 $m^2\ g^{-1}$. But most additives, on the contrary, tend to increase the particle size of the HTC carbon. For example, Na_2SO_4, NaCl, $NaNO_3$ and some organic additives, such cysteine and its derivatives, all would increase the particle size of the glucose derived HTC carbon from 100–200 nm to several micrometers.[22,25,26] These observations have led to many interesting processes for the synthesis of carbon microspheres with or without doping of heteroatoms, however, to our best knowledge, the influences of HTC additives on the following high temperature activation process have not yet been reported.

In this work, we report that HTC of glucose with NH_4Cl additive followed by KOH-activation can lead to N-doped activated carbon with significantly enhanced specific surface area,

College of Chemistry and Molecular Sciences, Hubei Key Laboratory of Electrochemical Power Sources, Wuhan University, Wuhan, 430072, P. R. China. E-mail: xbjin@whu.edu.cn

† Electronic supplementary information (ESI) available. See DOI: 10.1039/c6ra26141h

This journal is © The Royal Society of Chemistry 2017

Open Access Article. Published on 19 January 2017. Downloaded on 1/19/2026 6:30:39 PM.
This article is licensed under a Creative Commons Attribution 3.0 Unported Licence.

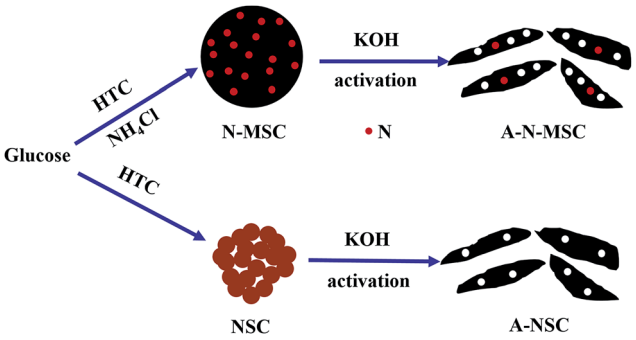

Scheme 1 Schematically shown the hydrothermal carbonization and activation process of glucose with and without the NH_4Cl additive.

despite the fact that the NH_4Cl additive will decrease the surface area of the HTC carbon as a result of formation of carbon microspheres. The difference between HTC with and without the NH_4Cl additive can be schematically shown in Scheme 1, where after activation, the NH_4Cl will lead to a more porous structure and N-doping of the activated carbon is indicated. The resulting activated carbon has a specific surface area exceeding 3000 $m^2\ g^{-1}$, and can deliver a specific capacity as high as 349 F g^{-1} at a current density of 1 A g^{-1} in 6 mol L^{-1} KOH.

2 Experimental section

2.1 Preparation of nanosphere carbon (NSC) and microsphere carbons (MSCs) through HTC

All chemical reagents in this work were of analytical purity and purchased from Sinopharm Chemical Reagent Company. High-purity deionized water (18.5 MΩ cm) was prepared by water purifier (Chengdu Pincheng Technology Co, Ltd.). Typically, 4 g glucose, a certain amount of NH_4Cl and 30 mL H_2O were added into a hydrothermal autoclave of 50 mL capacity, which was maintained at 190 °C for 5 h, and then cooled to room temperature naturally. After filtration and washing with absolute ethanol and deionized water several times (until the filtrate becomes clear), the solid product was collected and vacuum dried at 70 °C overnight. Without using NH_4Cl, the product is nanosphere carbon and denoted as NSC. The product of HTC with 2 g and 8 g NH_4Cl are microsphere carbons and denoted as N-MSC1 and N-MSC2 respectively. Using 0.15 mol HCl and 0.15 mol NaCl additives for the HTC of glucose also led to the generation of microsphere carbons, which are denoted as H-MSC and Na-MSC respectively.

2.2 Activation of the HTC carbons

The HTC carbons were impregnated with KOH with an alkali to carbon ratio of 3. After vacuum-dried at 75 °C overnight, the mixtures were heated (heating rate 10 °C min^{-1}) to 800 °C and maintained for 2 h under Ar flow. The resulting activated carbons were washed with 1 M HCl solution and double-distilled water, and dried overnight for characterization. The activated NSC, N-MSC1, N-MSC2, H-MSC and Na-MSC are denoted as A-NSC, A-N-MSC1, A-N-MSC2, A-H-MSC and A-Na-MSC respectively.

2.3 Characterizations

The structure and morphology of the samples were characterized by scanning electron microscopy (SEM, FEI Quanta 200), and high-resolution transmission electron microscopy (HRTEM, JEOL-2100), respectively. X-Ray photoelectron spectroscopy (XPS) analysis was carried out with a Thermo Fisher ESCALAB 250xi Ultra spectrometer with an Al Kα excitation source. Fourier-transform IR (FTIR) spectra of the samples were recorded using a Nicolet-MEXUS 670 Spectrophotometer. The pore structure of the samples was analysed by using a Micromeritics ASAP 2020 Analyzer (Norcross, GA) with nitrogen adsorption. The specific surface area was calculated using the Brunauer–Emmett–Teller (BET) method. Raman characterization was carried out using a RM-1000 Laser Confocal Raman Microspectroscopy (Renishaw, England) employing a 514.5 nm laser beam. Powder X-ray diffraction (XRD, Shimadzu XRD-6000 Cu Kα radiation) patterns were recorded between scattering angles (2θ) of 10–80°at a scanning rate of 4° min^{-1}.

2.4 Electrochemical measurements

The test electrodes were the nickel foam supported rolled membranes (dried in a vacuum oven at 110 °C before use) comprising 70 wt% active material and 15 wt% acetylene black plus 15 wt% polytetrafluoroethylene (PTFE). The mass load of the active material in an electrode was about 2.4 mg cm^{-2}. Cyclic voltammetry, galvanostatic charge–discharge curves in a 6 M KOH solution were recorded using a CHI660a potentiostat. For all electrochemical tests, a graphite plate and a Hg/HgO electrode were employed as the counter electrode and the reference electrode respectively, and degassing of the electrolyte was conducted by bubbling Ar for 15 min before each test.

3 Results and discussion

As shown in Fig. 1a, HTC of glucose without using any additive gave rise to nanosphere carbon (NSC) with particle sizes of about 200 nm. This sizes significantly increased to 2–3 μm (Fig. 1b) when 2 g NH_4Cl was added into the HTC reactor, and further increased to 4–5 μm (Fig. 1c) when 8 g NH_4Cl was added. The two microsphere carbons (MSCs) are denoted as N-MSC1 (2 g NH_4Cl) and N-MSC2 (8 g NH_4Cl) respectively. Apart from the great particle size difference between the MSCs and the NSC, the MSCs are black while the NSC presents a brown colour, suggesting that NH_4Cl can catalyse the dehydration carbonization of glucose, like other inorganic additives.[22,25] The catalytic role of NH_4Cl can also be evidenced by the oxygen contents in the N-MSCs, which were much lower than that in the NSC (Table S1†). On the other hand, as an electrolyte, the NH_4Cl might also induce flocculation and coagulation of carbonization products, leading to larger particle size of the HTC carbons.

Considering that the as obtained HTC carbons usually are low in specific surface area,[26] to obtain high surface area

Open Access Article. Published on 19 January 2017. Downloaded on 1/19/2026 6:30:39 PM.
This article is licensed under a Creative Commons Attribution 3.0 Unported Licence.

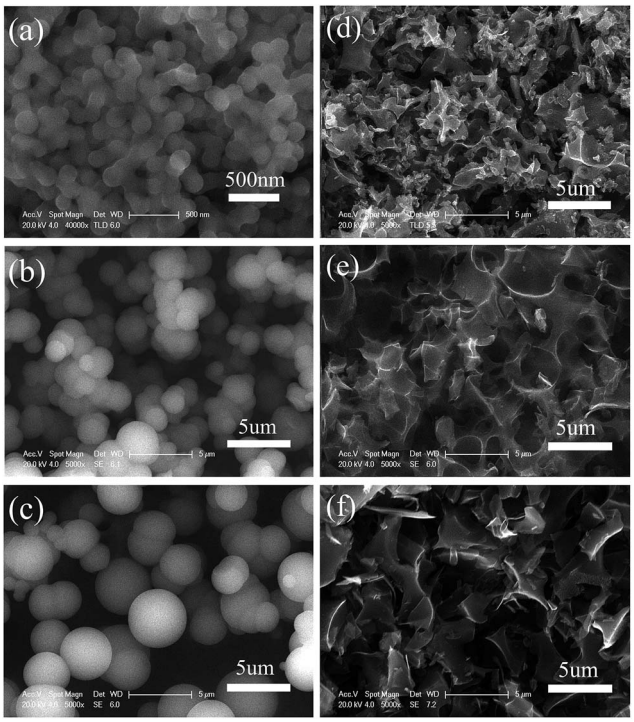

Fig. 1 SEM images of carbons generated by hydrothermal carbonization of 4 g glucose with or without using NH_4Cl additive. (a) NSC (0 g NH_4Cl); (b) N-MSC1 (2 g NH_4Cl); (c) N-MSC2 (8 g NH_4Cl). (d–f) SEM images of corresponding activated carbons: A-NSC (d), A-N-MSC1 (e) and A-N-MSC2 (f).

carbons, activation with KOH was performed at 800 °C, and the activated NSC, N-MSC1 and N-MSC2 are denoted as A-NSC, A-N-MSC1 and A-N-MSC2 respectively. The SEM images of these activated carbons are presented in Fig. 1 as well. It can be seen that after the activation, the spherical particles of the as obtained HTC carbons changed into many irregular carbon fragments. TEM images of the activated samples as exampled in Fig. 2 all indicate that there are plenty of micropores throughout the carbon fragments. In addition, XRD patterns (Fig. S1†) reveal these activated HTC carbons are in an amorphous feature, hence it can be concluded that activated carbons have been obtained after the KOH activation.

Fig. 3 shows the nitrogen adsorption–desorption isotherms of NSC, N-MSC1 and N-MSC2 before and after the activation. The NSC has a low specific surface area (11 $m^2 g^{-1}$), in line with previous reports.[26] The N-MSC1 and N-MSC2 exhibit much

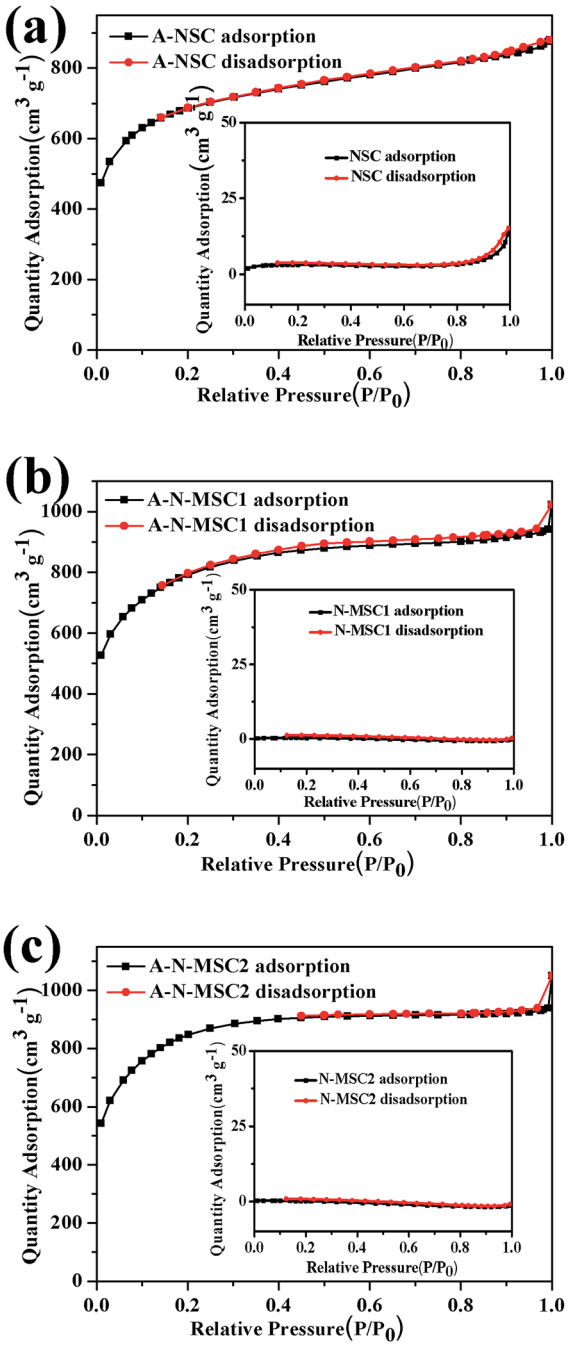

Fig. 3 BET N_2 gas sorption isotherms of different HTC carbons before and after the KOH activation as indicated.

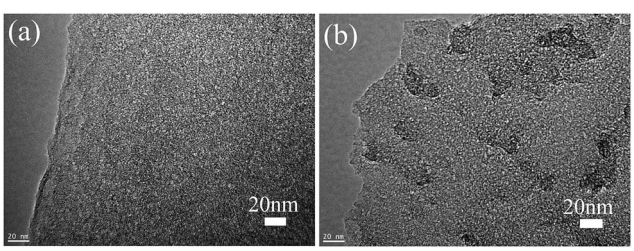

Fig. 2 TEM images of A-NSC (a) and A-N-MSC2 (b).

lower specific surface areas, 0.93 and 0.19 $m^2 g^{-1}$ respectively, obviously due to the larger particle size of the N-MSCs. As expected, all the activated HTC carbons have large specific surface areas according to BET tests. However, the specific surface areas of the A-N-MSC2 (3003 $m^2 g^{-1}$) and A-N-MSC1 (2795 $m^2 g^{-1}$) are significantly larger than that of A-NSC (2385 $m^2 g^{-1}$), although by intuition, the surface area of A-NSC, from the NSC precursor originally with a much higher surface area, was supposed to be higher than that of A-N-MSCs. Moreover, considering that the specific surface area of A-N-MSC2 is higher than that of A-N-

This journal is © The Royal Society of Chemistry 2017

Open Access Article. Published on 19 January 2017. Downloaded on 1/19/2026 6:30:39 PM.
This article is licensed under a Creative Commons Attribution 3.0 Unported Licence.

MSC1, it seems that the NH_4Cl additive for HTC of glucose played an important role in the pore generation during the activation. At the same time, microsphere carbons, namely H-MSC and Na-MSC have also been prepared by HTC of glucose at the presence of HCl and NaCl, respectively, and they both comprise carbon spheres with particle sizes similar to that of N-MSCs (Fig. S2†). However, after activation with KOH, the specific surface area of the activated H-MSC (A-H-MSC, 1789 m^2 g^{-1}) and Na-MSC (A-Na-MSC, 1630 m^2 g^{-1}) (Fig. S3†) are both significantly lower than that of A-NSC, agreeing with the intuition that the smaller the particle size of carbon precursor, the higher specific surface area of the activated resultant. In addition, the N_2 sorption behaviour of activated samples were more or less between type I and type II, which feature a mixture of high N_2 uptake at P/P_0 < 0.05 with continually increasing absorption at higher P/P_0 (0.05–0.5) for developed mesopores (Fig. 3). The detailed analysis indicates that the increased surface area of A-N-MSC2 over A-NSC is mainly arising from the mesopores 2–5 nm in sizes (Table S2 and Fig. S3b†), which would be in favor of electrolyte accessibility compared to the micropores surface area.

To identify the role of NH_4Cl additive in the whole process, X-ray photoelectron spectroscopy (XPS) analyses were carried out, with the elemental analysis listed in Table S1.† As shown in Fig. 4a, besides signal of C, the XPS survey spectrum of NSC shows an apparent signal of O with a content of about 22.3% (atomic ratio, the same below), which decreased significantly to about 7.1% in the N-MSC1 and 5.8% in N-MSC2, confirming the catalytic effect of NH_4Cl on the HTC of glucose. Obviously, NH_4Cl additive has led to the N doping of the HTC carbon, because the N-MSCs showed XPS signal of N but no signal of Cl. The N doping levels were about 2.8 at% and 4.2 at% in the N-MSC1 and N-MSC2 respectively. The high resolution N 1s spectra (Fig. 4b and c) indicate that the N species include pyridinic-N (398.5 eV), NH_2–N (399.4 eV), pyrrolic-N (400.1 eV) and graphitic-N (401 eV) respectively.[27–29] The C 1s spectra (Fig. S4†) also confirm the formation of C–N bonds in the N-MSCs,[30] and the more NH_4Cl added for the HTC, the more C–N bonds in the resulting carbon.

It is thus speculated that the high specific surface area of A-N-MSCs over that of A-NSC is due to the existence of doped N atoms in the N-MSCs, which caused extra pores during the activation. A possible explanation is that those nitrogenous groups are chemically more active than pristine carbon atoms, so there are more sites to be activated in the N doped HTC carbon. This can be evidenced by the XPS analyses. From Fig. 4a and d, it can be estimated that the N to C ratios in N-MSC1 and N-MSC2 are 0.035 and 0.053, and in A-N-MSC1 and A-N-MSC2 0.01 and 0.018 respectively, indicating that in comparison with pristine carbon sites, a larger percentage of N sites decomposed during the KOH activation. In detail, after the activation it can be seen that the NH_2–N signal disappeared and the contents of all the other three kinds of N, namely, pyridinic-N, pyrrolic-N, graphitic-N decreased significantly. These changes could also been evidenced by the FTIR spectra (Fig. S5†). For the N-MSCs, there is an apparent absorption band between 3000–3400 cm^{-1}, which can be linked to stretching vibrations of NH_2 and NH groups, and the corresponding bending mode of NH_2 occurs at 799 cm^{-1}.[31–33] There are also a series absorption peaks centred at 1620, 1382, 1250 and 1045 cm^{-1} respectively, which can be assigned to the stretching vibrations of C=N bonds and the aromatic C–N bonds.[33] However, all these absorptions disappear or can be hardly recognized in the FTIR spectra of the A-N-MSCs when compared to the spectrum of A-NSC, indicating that most of N atoms were removed during the KOH activation.

The removal of nitrogenous groups could result in extra defects in the AC. As shown in Fig. 5, the Raman spectra of A-NSC, A-N-MSC1 and A-N-MSC2 all display a D peak (signal of the defect- or disorder-induced scattering) at 1355 cm^{-1} and a G peak (signal of the vibration of sp^2-bonded carbon atoms) at

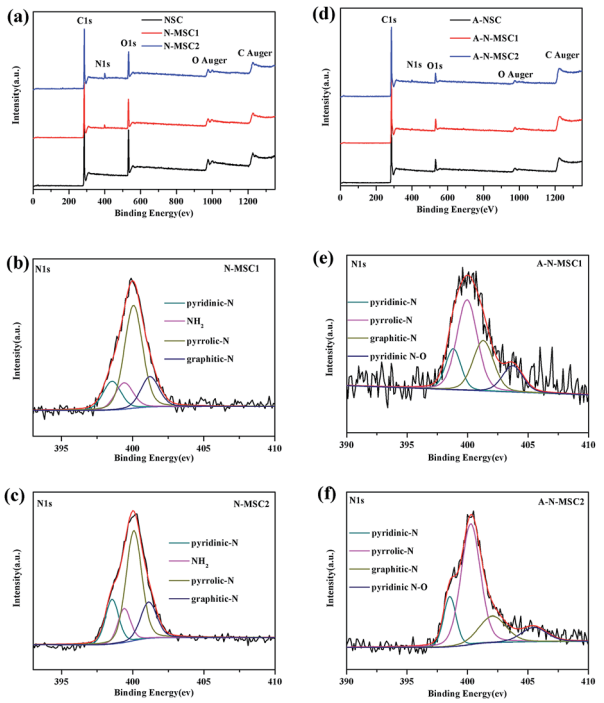

Fig. 4 XPS spectra of the HTC carbons before (a) and after (d) KOH activation at 800 °C. (b), (c), (e) and (f) display the corresponding high resolution N 1s peaks.

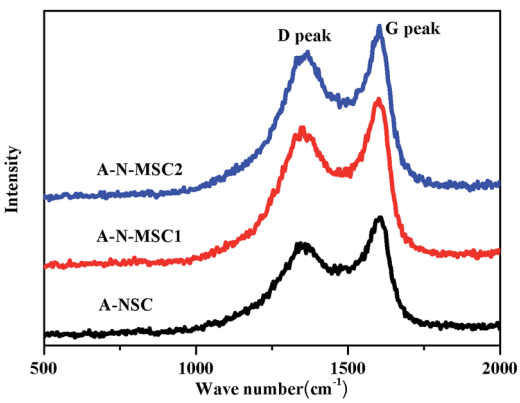

Fig. 5 Raman spectra of different activated HTC carbons as indicated.

Open Access Article. Published on 19 January 2017. Downloaded on 1/19/2026 6:30:39 PM.
This article is licensed under a Creative Commons Attribution 3.0 Unported Licence.

1595 cm^{-1}.[34] The intensity ratio of D peak to G peak (I_D/I_G) is an indicator of structural disorder in carbon materials, and the larger the I_D/I_G value, the more defects in a carbon. The I_D/I_G values for the A-NSC, A-N-MSC1 and A-N-MSC2 were calculated to be 0.80, 0.84, and 0.86 respectively, suggesting there are more disorders and defects in the A-N-MSC2, which is in line with the fact that the A-N-MSC2 is most rich in pores according to the BET analysis (Fig. 3).

The A-N-MSCs with a surface area exceeding 3000 $m^2\ g^{-1}$ could be high performance electrode materials for supercapacitors,[35–40] because the abundant micropores, mesopores and defects in the carbon may benefit the electrolyte transfer and exposure of reactive sites. In addition, there are about 1.7% N doping in the A-N-MSC2, among which the pyridinic-N, and pyrrolic-N could increase the pseudo-capacitance, and the graphitic-N could enhance the electronic conductivity.[29] Fig. 6a compares the cyclic voltammograms (CVs) of A-NSC, A-N-MSC1 and A-N-MSC2 at a scan rate of 20 mV s^{-1} in 6 M KOH. All the CVs show a rectangular-like shape, at the same time, the corresponding galvanostatic charge/discharge curves (Fig. 6b) between −1 V and 0 V (*vs.* the Hg/HgO reference electrode) at a current density of 1 A g^{-1}, exhibit a nearly triangular shape, indicating excellent capacitive behaviour. Obviously, the specific capacitances of the A-N-MSCs are much higher than that of A-NSC. The higher specific capacitance of A-N-MSC2 than A-N-MSC1 can be ascribed to the higher specific surface area and nitrogen content in the A-N-MSC2.

The rate performances of the three samples are compared in Fig. 6c. In line with previous reports, at current densities of 0.5 A g^{-1}, 1 A g^{-1} and 10 A g^{-1}, the A-NSC activated from the glucose derived carbon by HTC without NH_4Cl additive shows a specific capacitance of 294, 254, 211 F g^{-1} respectively.[41] The A-N-MSC2 is superior over the A-N-MSC1 and A-NSC at all the tested current densities for the charge/discharge, which delivers a specific capacitance of 390, 349 and 305 F g^{-1} at current densities of 0.5 A g^{-1}, 1 A g^{-1} and 10 A g^{-1} respectively, manifesting a significantly better supercapacitor performance than that of A-NSC.

The long-term cycling stability of A-N-MSC2 was also tested using galvanostatic charge/discharge at 10 A g^{-1} (Fig. 6d). The initial capacitance of A-N-MSC2 is about 305 F g^{-1}, which keeps fairly stable over the 10 000 cycles with a coulombic efficiency of about 100%. The capacitance at 10000th cycle is about 283 F g^{-1}, corresponding to a capacity retention of 92.8% with respect to the first discharge capacity, revealing an excellent cycling performance. The high specific capacitance, high rate performance and cycling stability of the A-N-MSC2 suggesting that hydrothermal carbonization of glucose with NH_4Cl additive followed by KOH activation is an efficient route to produce high performance capacitive carbon.

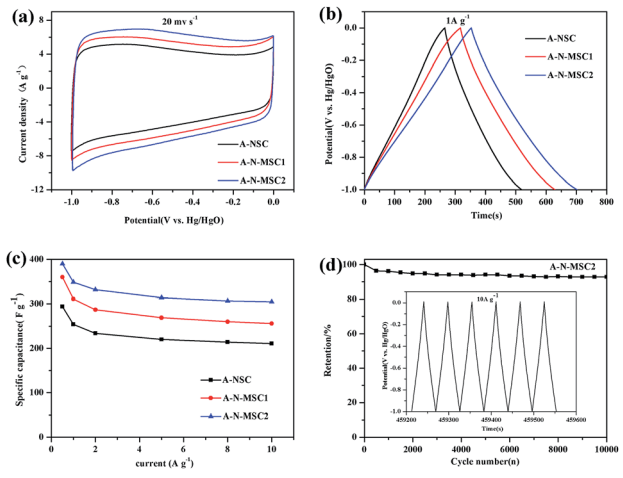

Fig. 6 Electrochemical performance of A-NSC, A-N-MSC1 and A-N-MSC2 in 6 mol L^{-1} KOH: (a) cyclic voltammograms at a scan rate of 20 mV s^{-1}, (b) galvanostatic charge/discharge curves at a current density of 1 A g^{-1}, (c) relationship between the specific capacitance and the current density for charge/discharge, and (d) cycling performance of A-N-MSC2 at a charge/discharge current density of 10 A g^{-1}, and the inset shows the 8000th to 8006th charge/discharge curves.

4 Conclusions

In summary, we demonstrated a simple route to convert glucose to highly porous nitrogen-doped carbons: hydrothermal carbonization at the presence of NH_4Cl, followed by KOH activation at 800 °C. It was found that the NH_4Cl additive can catalyse the hydrothermal carbonization of glucose and change the product form nanosphere carbon (NSC, ~200 nm in particle size) to nitrogen doped microsphere carbons (N-MSC, several micrometers in particle size), but after the following activation, the A-N-MSC shows a specific surface area (exceeding 3000 $m^2\ g^{-1}$) greatly higher than that of A-NSC (2385 $m^2\ g^{-1}$). The extra pores and/or defects generated in the A-N-MSC can be ascribed to the chemical etching of nitrogenous groups. The feed ratio between the NH_4Cl and glucose for the hydrothermal carbonization has an important influence on the surface area and N-doping level of the A-N-MCS. In 6 M KOH, the A-N-MSC can deliver a specific capacitance of 349 and 311 F g^{-1} in 6 M KOH at 1 A g^{-1}, significantly higher than 254 F g^{-1} of the A-NSC. The A-N-MSC also shows high rate performance and high cycling stability. Our findings promise an efficient route to prepare highly porous N-doped carbon with high capacitive performance.

Acknowledgements

This work is supported by NSFC (21173161, 21673164) and the Large-scale Instrument and Equipment Sharing Foundation of Wuhan University.

References

1 M. Jordá-Beneyto, D. Lozano-Castelló, F. Suárez-García, D. Cazorla-Amorós and Á. Linares-Solano, *Microporous Mesoporous Mater.*, 2008, **112**, 235–242.
2 M. Zyzlila Figueroa-Torres, A. Robau-Sánchez, L. De la Torre-Sáenz and A. Aguilar-Elguézabal, *Microporous Mesoporous Mater.*, 2007, **98**, 89–93.
3 C. P. Huang and M. H. Wu, *Water Res.*, 1977, **11**, 673–679.

 This journal is © The Royal Society of Chemistry 2017

Open Access Article. Published on 19 January 2017. Downloaded on 1/19/2026 6:30:39 PM.
This article is licensed under a Creative Commons Attribution 3.0 Unported Licence.

4 M. Goyal, V. K. Rattan, D. Aggarwal and R. C. Bansal, *Colloids Surf., A*, 2001, **190**, 229–238.
5 A. Perrin, A. Celzard, J. F. Marêché and G. Furdin, *Carbon*, 2004, **42**, 1249–1256.
6 F. Rodríguez-Reinoso, Y. Nakagawa, J. Silvestre-Albero, J. M. Juárez-Galán and M. Molina-Sabio, *Microporous Mesoporous Mater.*, 2008, **115**, 603–608.
7 Q.-Y. Li, H.-Q. Wang, Q.-F. Dai, J.-H. Yang and Y.-L. Zhong, *Solid State Ionics*, 2008, **179**, 269–273.
8 P. Guo, Y. Gu, Z. Lei, Y. Cui and X. S. Zhao, *Microporous Mesoporous Mater.*, 2012, **156**, 176–180.
9 Roskill Report, http://www.roskill.com/reports/industrial-minerals/activated-carbon, 2008, accessed 26 August, 2016.
10 M. M. Titirici, A. Thomas and M. Antonietti, *Adv. Funct. Mater.*, 2007, **17**, 1010–1018.
11 C. Falco, F. Perez Caballero, F. Babonneau, C. Gervais, G. Laurent, M.-M. Titirici and N. Baccile, *Langmuir*, 2011, **27**, 14460–14471.
12 C. Falco, J. M. Sieben, N. Brun, M. Sevilla, T. van der Mauelen, E. Morallon, D. Cazorla-Amoros and M. M. Titirici, *ChemSusChem*, 2013, **6**, 374–382.
13 N. Baccile, G. Laurent, F. Babonneau, F. Fayon, M.-M. Titirici and M. Antonietti, *J. Phys. Chem. C*, 2009, **113**, 9644–9654.
14 B. M. Kabyemela, T. Adschiri, R. M. Malaluan and K. Arai, *Ind. Eng. Chem. Res.*, 1999, **38**, 2888–2895.
15 M. Sevilla and A. B. Fuertes, *Chem.–Eur. J.*, 2009, **15**, 4195–4203.
16 L. Wei and G. Yushin, *Nano Energy*, 2012, **1**, 552–565.
17 M. J. Munoz-Guillena, M. J. Illan-Gomez, J. M. Martin-Martinez, A. Linares-Solano and C. Salinas-Martinez de Lecea, *Energy Fuels*, 1992, **6**, 9–15.
18 J. Alcanizmonge, D. Cazorlaamoros, A. Linaressolano, S. Yoshida and A. Oya, *Carbon*, 1994, **32**, 1277–1283.
19 D. Lozano-Castelló, M. A. Lillo-Ródenas, D. Cazorla-Amorós and A. Linares-Solano, *Carbon*, 2001, **39**, 741–749.
20 Y. Zhu, S. Murali, M. D. Stoller, K. J. Ganesh, W. Cai, P. J. Ferreira, A. Pirkle, R. M. Wallace, K. A. Cychosz, M. Thommes, D. Su, E. A. Stach and R. S. Ruoff, *Science*, 2011, **332**, 1537–1541.
21 M.-M. Titirici, M. Antonietti and N. Baccile, *Green Chem.*, 2008, **10**, 1204–1212.
22 J. Ming, Y. Wu, G. Liang, J.-B. Park, F. Zhao and Y.-K. Sun, *Green Chem.*, 2013, **15**, 2722–2726.
23 T.-P. Fellinger, R. J. White, M.-M. Titirici and M. Antonietti, *Adv. Funct. Mater.*, 2012, **22**, 3254–3260.
24 N. Fechler, S.-A. Wohlgemuth, P. Jäker and M. Antonietti, *J. Mater. Chem. A*, 2013, **1**, 9418–9421.
25 K. Latham, G. Jambu, S. Joseph and S. Donne, *ACS Sustainable Chem. Eng.*, 2014, **2**, 755–764.
26 S.-A. Wohlgemuth, F. Vilela, M.-M. Titirici and M. Antonietti, *Green Chem.*, 2012, **14**, 741–749.
27 J. R. Pels, F. Kapteijn, J. A. Moulijn, Q. Zhu and K. M. Thomas, *Carbon*, 1995, **33**, 1641–1653.
28 H. Wang, T. Maiyalagan and X. Wang, *ACS Catal.*, 2012, **2**, 781–794.
29 L. Sun, L. Wang, C. Tian, T. Tan, Y. Xie, K. Shi, M. Li and H. Fu, *RSC Adv.*, 2012, **2**, 4498–4506.
30 Z.-H. Sheng, L. Shao, J.-J. Chen, W.-J. Bao, F.-B. Wang and X.-H. Xia, *ACS Nano*, 2011, **5**, 4350–4358.
31 T. Ramanathan, F. T. Fisher, R. S. Ruoff and L. C. Brinson, *Chem. Mater.*, 2005, **17**, 1290–1295.
32 S. Hwang, S. Lee and J.-S. Yu, *Appl. Surf. Sci.*, 2007, **253**, 5656–5659.
33 D. Zhang, Y. Hao, Y. Ma and H. Feng, *Appl. Surf. Sci.*, 2012, **258**, 2510–2514.
34 P. K. Chu and L. Li, *Mater. Chem. Phys.*, 2006, **96**, 253–277.
35 D. Hulicova, J. Yamashita, Y. Soneda, H. Hatori and M. Kodama, *Chem. Mater.*, 2005, **17**, 1241–1247.
36 B. Xu, S. Hou, G. Cao, F. Wu and Y. Yang, *J. Mater. Chem.*, 2012, **22**, 19088–19093.
37 B. Xu, H. Duan, M. Chu, G. Cao and Y. Yang, *J. Mater. Chem. A*, 2013, **1**, 4565–4570.
38 X. Wu, L. Jiang, C. Long and Z. Fan, *Nano Energy*, 2015, **13**, 527–536.
39 C. Long, J. Zhuang, Y. Xiao, M. Zheng, H. Hu, H. Dong, B. Lei, H. Zhang and Y. Liu, *J. Power Sources*, 2016, **310**, 145–153.
40 F. Sun, J. Gao, Y. Yang, Y. Zhu, L. Wang, X. Pi, X. Liu, Z. Qu, S. Wu and Y. Qin, *Carbon*, 2016, **109**, 747–754.
41 D. Yuan, J. Chen, J. Zeng and S. Tan, *Electrochem. Commun.*, 2008, **10**, 1067–1070.